Structure

Artificial neural networks for solution scattering data analysis

Graphical abstract

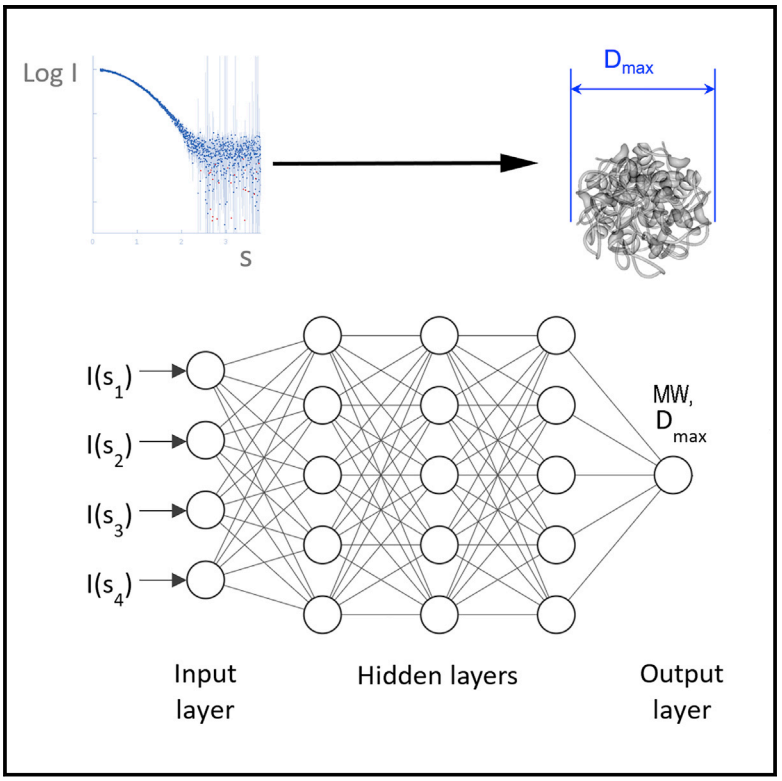

Highlights

- A method based on the application of feedforward neural networks is presented
- It allows the prediction of molecular weights and maximum distances from SAXS data
- Applicable to data from folded, intrinsically disordered proteins and nucleic acids
- It yields higher accuracy and better robustness compared to existing methods

Authors

Dmitry S. Molodenskiy, Dmitri I. Svergun, Alexey G. Kikhney

Correspondence

svergun@embl-hamburg.de (D.I.S.), a.kikhney@embl-hamburg.de (A.G.K.)

In brief

Molodenskiy et al. propose a method for primary SAXS data analysis that can predict molecular weight and maximum intraparticle distance directly from experimental data with higher accuracy and better robustness against simulated experimental noise compared to existing methods.

Molodenskiy et al., 2022, Structure *30*, 900–908
June 2, 2022
https://doi.org/10.1016/j.str.2022.03.011

CellPress

CellPress
OPEN ACCESS

Structure

Resource

Artificial neural networks for solution scattering data analysis

Dmitry S. Molodenskiy,[1,2] Dmitri I. Svergun,[1,*] and Alexey G. Kikhney[1,*]
[1]European Molecular Biology Laboratory, Hamburg Site, EMBL c/o DESY, Notkestrasse 85, 22607 Hamburg, Germany
[2]Lead contact
*Correspondence: svergun@embl-hamburg.de (D.I.S.), a.kikhney@embl-hamburg.de (A.G.K.)
https://doi.org/10.1016/j.str.2022.03.011

SUMMARY

Small-angle X-ray scattering (SAXS) experiments are widely used for the characterization of biological macromolecules in solution. SAXS patterns contain information on the size and shape of dissolved particles in nanometer resolution. Here we propose a method for primary SAXS data analysis based on the application of artificial neural networks (NNs). Trained on synthetic SAXS data, the feedforward NNs are able to reliably predict molecular weight and maximum intraparticle distance (D_{max}) directly from the experimental data. The method is applicable to data from monodisperse solutions of folded proteins, intrinsically disordered proteins, and nucleic acids. Extensive tests on synthetic SAXS data generated in various angular ranges with varying levels of noise demonstrated a higher accuracy and better robustness of the NN approach compared to the existing methods.

INTRODUCTION

Small-angle X-ray scattering (SAXS) from biological macromolecules in solution is a powerful technique providing information on supermolecular structures and dynamics under a wide range of conditions (Gräwert and Svergun, 2020; Guinier and Fournet, 1955; Svergun et al., 2013). Due to non-restrictive requirements to sample preparation for SAXS experiments and recent progress in the instrumentation and of data analysis methods (Hopkins et al., 2017; Liu et al., 2012; Manalastas-Cantos et al., 2021), the method is widely utilized also in high throughput studies.

The SAXS data are obtained by illuminating a dilute, typically monodisperse solution of macromolecules with a monochromatic X-ray beam that results in an isotropic two-dimensional (2D) scattering pattern. The latter is azimuthally integrated into a 1D scattering profile that represents the scattering intensity I(s) as a function of the scattering vector $s = 4\pi\sin\theta/\lambda$, where θ is the half of the angle between incoming and diffracted beams, and λ is the X-ray wavelength. The "background" scattering from the pure solvent is independently measured and subtracted from that of the solution. From the background-subtracted scattering profile, one can directly evaluate structural characteristics of the scattering particle: radius of gyration (R_g), maximum intraparticle distance (D_{max}), pair distance distribution function (p(r)), and molecular weight (MW). It is further possible to reconstruct the overall shape *ab initio* or obtain a hybrid model employing structural information from the high-resolution methods.

There are a number of established methods for the estimation of MW from SAXS data on a relative scale (i.e., without relying on scattering from calibrants). The accuracy of these estimates is limited (in the range of about 10%) (Hajizadeh et al., 2018). These methods have been developed primarily for globular proteins, and their applicability to SAXS data from disordered proteins and nucleic acids is not straightforward. Here, we explore the use of artificial neural networks (NN) for the primary SAXS data analysis to assess the MW and D_{max} directly from the scattering data from folded proteins, intrinsically disordered proteins (IDP), and nucleic acids.

Recently, the application of NNs has experienced a sudden leap in almost all areas of everyday life, also thanks to the development of deep learning technologies (Schmidhuber, 2015). Massive progress has happened in many biological applications as well, including bioinformatics (Armenteros et al., 2019), a recent breakthrough in *in silico* protein folding by AlphaFold (Jumper et al., 2021), and even in the area of SAXS shape reconstruction (He et al., 2020).

NNs are excellent tools for supervised learning; the task of learning is to find a function that maps an input to the desired output based on a training dataset. In our case, the input is a vector of experimental intensities I(s) on a relative scale, and the output could be a value representing an overall geometrical parameter, e.g., the MW or D_{max}. Since obtaining reliable experimental SAXS data in sufficient quantities is challenging, one could compute the scattering from known protein and/or nucleic acid models for training assuming that the mapping function would be applicable to experimental data.

The simulated training set can be augmented: this way, one can easily adjust the area of applicability of, for example, a given NN model and tailor it for the specific objects, instrumentation features, or experimental setup. One example from the SAXS area is the robustness of predictions against experimental noise,

which is inevitably present in the experimental SAXS data and reduces its information content, thus increasing the ambiguity of data interpretation.

We employed several feedforward artificial NNs trained on noise-augmented synthetic SAXS data generated from thousands of experimentally determined models to estimate MW and D_{max} from folded proteins, unfolded proteins, and nucleic acids. Here we demonstrate that our method has higher accuracy and is less demanding in terms of data quality compared to the well-established methods to assess MW for folded proteins and nucleic acids. To the best of our knowledge, our method is unique for the MW estimation from SAXS data of IDP. Our method can also reliably estimate the maximum intraparticle distance D_{max} directly from the SAXS profile for the aforementioned macromolecule types.

Estimation of the MW from SAXS data

The approaches for MW estimation can be divided into two major categories: concentration-dependent and concentration-independent methods. The first category exploits the dependence of the forward scattering I(0) on the total number of electrons in the irradiated molecule (and, thus, on MW) and relies on the scattering from calibrants, e.g., from water or a protein with known MW (Mylonas and Svergun, 2007). These methods require the knowledge of sample concentration, partial specific volume, and scattering contrast of the solute. The second category utilizes a single background-subtracted profile on a relative scale and requires no additional information. Concentration-independent methods are more convenient to use, and moreover, in some cases, the solute concentration cannot be accurately measured (e.g., for in-line size-exclusion chromatography SAXS experiments). Below we shall focus on concentration-independent methods.

Porod's method

The historically first concentration-independent method is the so-called Porod's method (Porod, 1951). It is based on the fundamental properties of the Fourier transform known as the Parseval theorem:

$$\int_0^\infty s^2 I(s) ds = 2\pi^2 \int_V (\Delta\rho(r))^2 dV = Q \qquad \text{(Equation 1)}$$

where s is the scattering vector, I(s) is the intensity of the scattered radiation, $\Delta\rho$ is excess electron density, and Q is the Porod invariant. If we consider the scattering particle to be of homogeneous electron density, the right part of the Equation (1) simplifies to the following:

$$Q = 2\pi^2 \Delta\rho^2 V. \qquad \text{(Equation 2)}$$

Given that intensity in the origin equals $I(0) = (\Delta\rho)^2 V^2$,

$$V = 2\pi^2 I(0)/Q. \qquad \text{(Equation 3)}$$

The MW is typically estimated as an empirical relation between the volume of the particle and its mass, which in the case of folded proteins is about MW/V $\approx$ 0.625 (Petoukhov et al., 2012). This calculation is limited by the three factors: (1) integration in Equation (1) cannot be performed due to limitations in real experimental s-range, assuming globular proteins $I \sim s^{-4}$ power law is usually applied to extrapolate the intensities on higher angles; (2) the integration is affected by the experimental noise and the accuracy of background subtraction; and (3) Equation (2) implies homogeneity of the scattering particle.

SAXSMoW method

The Porod's invariant approach was extended by Fischer et al. (2010) and Piiadov et al. (2019). Here, the authors integrate the Porod invariant in Equation (1) not up to infinity, but up to a fixed s_{max} value:

$$Q' = \int_0^{s_{max}} s^2 I(s) ds. \qquad \text{(Equation 4)}$$

The authors introduce the so-called apparent volume as $V' = 2\pi^2 I(0)/Q'$ (similar to Equation (3)), and establish a linear dependence between V and V':

$$V = A + BV', \qquad \text{(Equation 5)}$$

where the coefficients A and B are determined empirically for different s_{max} values from simulated protein SAXS data. Given the lookup table with A and B values, one can find these coefficients corresponding to the experimental s_{max} and obtain a more accurate prediction for the MW.

Volume of correlation

Another approach was developed by Rambo and Tainer (2013) and introduces the so-called volume of correlation:

$$V_c = \frac{I(0)}{\int_0^\infty sI(s) ds}. \qquad \text{(Equation 6)}$$

The authors found an empirical dependence between V_c and the MW:

$$MW = \left(\frac{V_c^2/R_g}{e^c}\right)^{1/k}, \qquad \text{(Equation 7)}$$

where c and k are empirically determined constants via fitting results from theoretical scattering profiles. The authors mentioned $e^c = 0.1231$ and $1/k = 1$ for proteins and $e^c = 0.00934$ and $1/k = 0.808$ for RNA. Thus, this approach is applicable not only to SAXS data from proteins but to RNA data as well.

Machine learning methods

The web server for rapid search of structural neighbors DARA (Kikhney et al., 2016) accepts SAXS data from proteins, nucleic acids, or their complexes, finds the closest SAXS profiles precomputed from PDB (Berman et al., 2000) models, and reports the MW and D_{max} of these models. If there is a structural neighbor that fits well the experimental data, then these values can be used as the estimates of the overall structural parameters.

The size&shape method (Franke et al., 2018) allows for a fast and selective lookup of structural neighbors in a database of SAXS patterns precomputed from geometrical bodies and

protein models from the PDB. This approach enables rapid multiclass shape classification (compact, extended, random-chain, etc.) and estimation of D_{max} and MW directly from the experimental SAXS data from proteins.

Bayesian assessment of protein MW

In a recent method (Hajizadeh et al., 2018), the MW is estimated using Bayesian inference with the MW calculations from the aforementioned methods. The authors simulated a large test dataset of SAXS profiles, then calculated the MW for each profile using each method to build a probability distribution, which describes the original probability of obtaining a particular calculated MW given the true molecular weight. These probabilities are combined across all methods, and the most likely MW is thus estimated. The advantage of the method is that it employs all other methods and provides the most probable MW alongside its credibility interval. The disadvantage is similar to the shape&-size method; the assessment works only for compact proteins.

Estimation of the maximum intraparticle distance Dmax from SAXS data

The assessment of the maximum size D_{max} utilizes a pair distance distribution function p(r), which is a histogram of distances between pairs of points in the particle, weighted by the product of their scattering contrasts (Guinier and Fournet, 1955). Mathematically, the p(r) function is closely related to the scattering intensity I(s) via the spherically averaged Fourier transformation (Debye, 1915):

$$I(s) = \int_0^{D_{max}} p(r)\frac{\sin(sr)}{sr}dr \qquad \text{(Equation 8)}$$

$$p(r) = \frac{r}{2\pi^2}\int_0^{\infty} sI(s)\sin(sr)ds \qquad \text{(Equation 9)}$$

(here, $p(r) = 0$ for $r > D_{max}$). The limited angular range of the experimental data, as well as the presence of experimental noise, make the evaluation of p(r) an ill-posed problem. The method of solving this problem by an indirect Fourier transformation (IFT) has been originally proposed by Glatter (1977), and further developed by Svergun (1992) and Vestergaard and Hansen (2006). Here D_{max} must be provided as an input parameter, and the p(r) function is expressed as a sum of analytical functions (e.g., cubic splines). Finally, a regularization procedure (Tikhonov and Arsenin, 1977) is applied to calculate the p(r) agreeing with experimental data satisfying additional constraints. The most common constraint is the smoothness of the p(r), so termination effects are reduced as much as possible. However, in these approaches, the choice of the final solution remains a subjective criterion left to the discretion of the user.

In the program AUTOGNOM (Petoukhov et al., 2007) (presently DATGNOM), multiple runs of GNOM (Svergun, 1992) are performed with D_{max} values ranging from $2R_g$ to $4R_g$ to find the optimum D_{max} and provide the p(r) function. Here R_g is the radius of gyration from the Guinier approximation.

RESULTS AND DISCUSSION

Training/validation/test sets

In this study, we considered three types of biological macromolecules: folded proteins, IDPs, and nucleic acids. To construct a training set, we have utilized experimentally determined atomic models of the macromolecules available from respective databases. Each model was examined for connectivity, and models with domains separated by more than 7 Å were excluded. Heteroatoms were removed from all models.

Folded proteins

A total of 135,238 atomic coordinate files describing protein structures from protein-only biological assemblies were obtained from the Protein Data Bank (PDB) (Berman et al., 2000). 99% of these models have MW below 450 kDa; 80% of the models are in the range 10–86 kDa. To avoid bias toward smaller proteins, we have constructed a histogram of MW distribution for the pool of models. For each bin of this histogram, we have selected an equal number of models, so R_g values were evenly distributed within each bin. The selected 6,855 models contained both compact and extended proteins with MW in the range 4–410 kDa, R_g in the range 1–14.6 nm, and D_{max} in the range 3–51 nm.

Intrinsically disordered proteins

To prepare a set of IDP models, we used the Protein Ensemble Database for intrinsically disordered proteins (PED) (Lazar et al., 2021). A snapshot of the database was made that included 172 depositions and 269 ensembles, each ensemble containing between 3 and 29,598 models. We have used up to 50 conformers from each ensemble resulting in a total of 10,089 models. The selected pool of models contained IDPs with MW in the range 0.6–92.6 kDa, R_g in the range 0.5–13.5 nm, and D_{max} in the range 1.2–41.3 nm.

Nucleic acids

For the DNA and RNA models, we used the NDB server (Coimbatore Narayanan et al., 2014). A total of 2,864 DNA-only and RNA-only models were obtained with MW in the range 0.5–314 kDa, R_g in the range 0.7–6.8 nm, and D_{max} in the range 1.9–21.5 nm.

Preparing the simulated SAXS data

Theoretical scattering curves were computed on the absolute scale with CRYSOL 2.8 (Barberato et al., 1995) from ATSAS 3.0.3 in the range of momentum transfer from s = 0 to s = 1.0 $Å^{-1}$ on a grid of 256 points using 99 spherical harmonics. The experimental noise at seven different protein concentrations, c = 0.25, 0.5, 1, 2, 4, 8, and 16 mg/mL, was simulated based on experimental data from the EMBL's P12 beamline (Blanchet et al., 2015). This corresponded to the data acquired with the sample-to-detector distance of 3 m, total exposure time of 1 s, and X-ray energy of 10 keV. No structure factor or polydispersity was simulated. The augmented SAXS profiles were normalized to I(0) = 1, and the examples of the simulated data are shown in Figure 1. The ground truth values of MW and D_{max} were calculated from the models by CRYSOL. We routinely used GNU parallel (Tange, 2018) to speed up the calculations.

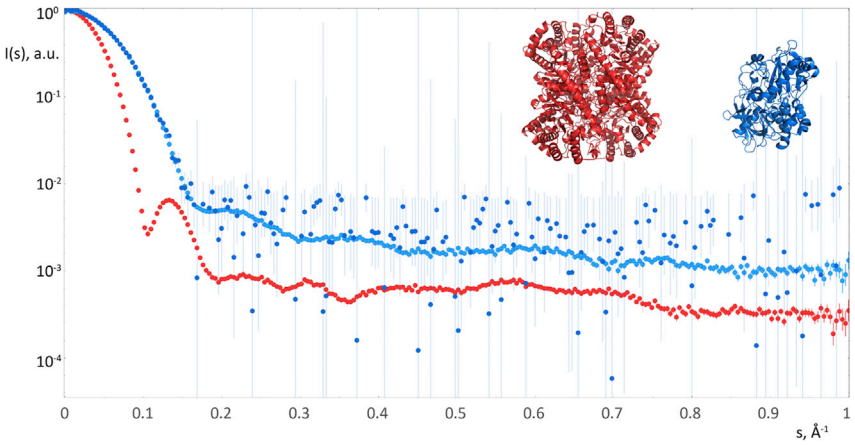

Figure 1. Examples of noise-augmented simulated data from the training set

Red dots: SAXS data computed from xylose isomerase (red model, PDB: 1a0d, MW = 198 kDa, D_{max} = 101.5 Å), concentration 16 mg/mL. Blue dots: data computed from oxidoreductase (blue model, PDB: 3b3r, MW = 55.7 kDa, D_{max} = 79.1 Å); light blue dots correspond to the concentration 16 mg/mL, and dark blue dots correspond to 0.5 mg/mL.

Neural networks architecture

A feedforward NN consists of "dense" layers of interconnected units, and each unit of each layer is connected to all units of the next layer (Figure 2). A unit essentially performs a multiple linear regression operation, applies some activation function, and passes the result further to the next layer. Given an input vector $\vec{X}$, the unit does a dot multiplication of that vector with an internally stored vector of "weights" of the same dimensionality and (optionally) adds a scalar value. The output of the operation reads as follows:

$$out = f\left(\vec{X} \cdot \vec{w} + b\right), \qquad \text{(Equation 10)}$$

where w is the array of weights associated with the unit, b is the scalar ("bias"), and f is an analytical activation function. In this study, we considered two activation functions: "rectified linear unit" (ReLU) and hyperbolic tangent (tanh).

An NN contains an input layer, an output layer, and one or more hidden layers (Figure 2). Here, the number of the units of the input layer corresponds to the number of angular intensity points I(s) in the training set data (the experimental uncertainties were not used for training). Since we expect the NN models to predict either MW or D_{max}, the output layer consists of a single unit. The minimization algorithm optimizes the weights and biases of all units, so the output layer value becomes as close as possible to the "ground truth" values associated with the input data. This discrepancy is measured by a loss function; here, we used the mean absolute percentage error. Once trained, the NN can be used for predicting the desired parameters from previously unseen input data.

To avoid overfitting—when a NN learns the training set too well and tries to fit specific, non-general features of the training set—a separate validation dataset was prepared. During training, the performance of NN is evaluated by applying the loss function to the validation set. Each simulated dataset was randomly split into 80% training set and 10% validation set. The remaining 10% (test set) was used to benchmark the results against other methods.

To find the optimal architecture, we tried different numbers of units and hidden layers to accurately predict MW and D_{max}. The minimal architecture for the MW prediction was just one hidden layer with five units, whereas for D_{max} prediction, three layers with up to 80 units each were necessary.

Various preprocessing normalizations were tested for input I(s) data and output MW or D_{max} values. A simple condition I(0) = 1 was found optimal for MW determination; additional subtraction of the mean training set SAXS profile improved the results for D_{max}. In both cases, the output values were normalized by the maximum value in the set.

Initially, six NNs were trained (three types of biological macromolecules, for MW and D_{max}) on the angular range up to 1.0 $Å^{-1}$ using smooth data. The accuracy and robustness of MW/D_{max} predictions were investigated by re-training the NNs using noisy data and different angular ranges.

In this work, we used the TensorFlow software library with Keras interface (Abadi et al., 2016) in Python. For benchmarking

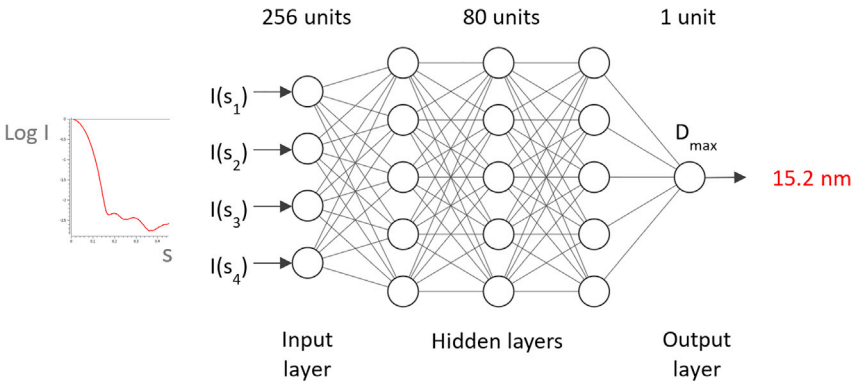

Figure 2. The architecture of the neural networks trained for MW/Dmax estimation (an example for D_{max} is shown)

Table 1. Performance of the neural networks trained on smooth data and applied on smooth test sets: average and median relative errors

	MW average	MW median	D_{max} average	D_{max} median
Folded proteins	2.50%	1.87%	2.78%	2.13%
IDPs	3.94%	2.37%	8.52%	4.15%
Nucleic acids	2.86%	2.00%	2.82%	1.89%

the NNs against other methods, we used the DATMW from ATSAS 3.0.3 (Hopkins et al., 2017; Liu et al., 2012; Manalastas-Cantos et al., 2021).

Application to the experimental data

To prepare the input data for the format of the NNs, the further steps are required:

1. estimate I(0) from the Guinier approximation using AUTORG (Petoukhov, 2007);
2. normalize the data to I(0) = 1;
3. convert to $Å^{-1}$ if necessary; rebin to the grid of the training set.

The angular range of the input SAXS data must match the range used for NN training. The sample type (folded protein/IDP/nucleic acid) must match the applied NN type.

Prediction accuracy

To evaluate the performance on the simulated test set data and experimental data from SASBDB (Kikhney et al., 2019), an average relative error was used as a metric of the prediction accuracy:

$$\langle \Delta_{rel} \rangle = \frac{1}{N} \sum_i \frac{|P_i - GT_i|}{GT_i}, \qquad \text{(Equation 11)}$$

where N is the total number of models in the test set, P is the predicted value (either MW or D_{max}), and GT is the ground truth value. The GT values were parsed from CRYSOL log files; for D_{max} the "envelope diameter" was taken since it takes into account the additional thickness of the hydration layer. In addition to the average, we computed the median relative error to control for the skewness of the error distribution.

For NNs trained on smooth (i.e., without added noise) data up to s_{max} = 1.0 $Å^{-1}$ and applied to the smooth test sets, we obtained the results presented in Table 1. For folded proteins, the plots of the predicted values versus ground truth values are shown in Figure 3.

Angular range

An important question arises: given the maximum angle s_{max}, what is the maximum precision of MW and D_{max} predictions that one can expect? The use of NNs enables a convenient opportunity to get a deeper insight into the information content of different angular ranges of the SAXS profiles. To evaluate the impact of the angular range on the accuracy of the MW and D_{max} predictions, we retrained the same NNs on smooth data computed from the folded proteins up to various s_{max} values, namely 0.8, 0.6, 0.4, 0.3, 0.2, 0.1, 0.05, and 0.025 $Å^{-1}$.

For the data cropped at s_{max} = 0.1 $Å^{-1}$, the accuracy of D_{max} predictions was 3.3%; it improves up to 2.8% with the angular range increased up to $s_{max} = 0.4^{-1}$ (see Figure 4, purple circles), but the further increase of the angular range did not affect the accuracy of the D_{max} predictions. That illustrates the fact that lower angles in reciprocal space contain information on the larger distances in real space.

For MW prediction the impact of higher angles was more pronounced: the accuracy improves from 8% to 2.8% with s_{max} increasing from 0.1 to 0.6 $Å^{-1}$ (see Figure 4, green circles). This is an interesting observation reflecting the fact that the curves normalized to I(0) = 1 were utilized in the training, so the direct information about the MW was effectively lost. The network was trained "indirectly" through the geometry of the curve, e.g., the Parseval theorem relations in Equations (1–3). As seen from Figure 4, the intensities at

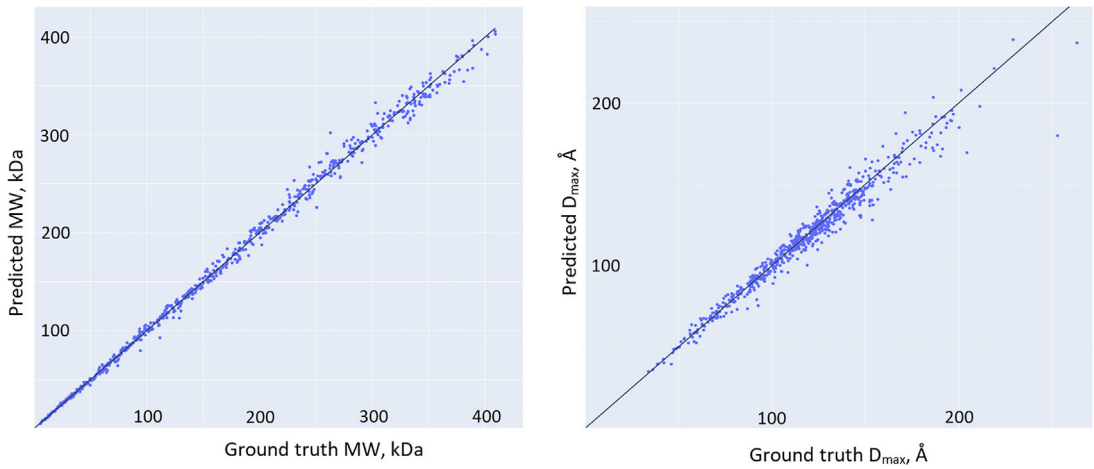

Figure 3. Predictions from 684 test data sets simulated from folded protein models (without added noise) versus ground truth. Left: molecular weight (MW); right: maximum intraparticle distance (D_{max}). Lines of equality are in black.

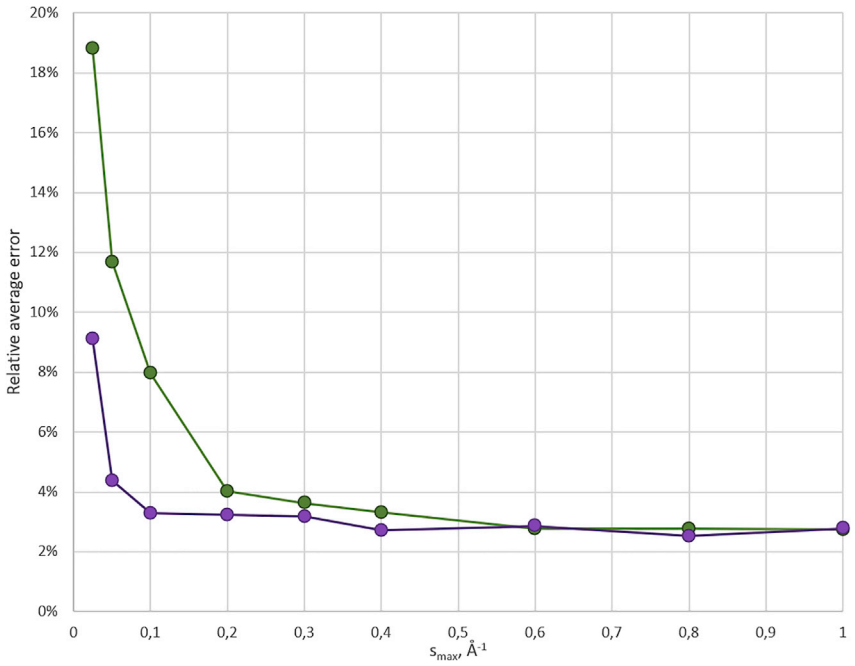

Figure 4. Relative average MW error (green) and D_{max} error (purple) estimated from smooth data decreases with increasing angular range

higher angles do provide important information contributing to the overall estimation of the MW.

Effects of the experimental noise

Depending on the sample concentration, contrast, molecule volume, and intensity of the X-ray beam, the noise in I(s) may vary drastically. To evaluate how the amount of noise impacts the prediction accuracy, we have added simulated noise to the folded proteins test dataset (with known ground truth MW and D_{max}) and first applied the aforementioned NNs trained on the smooth data up to s_{max} = 1.0 Å^{-1}.

For simulated concentrations 4, 8, and 16 mg/mL, the average relative MW error was below 3%, i.e., comparable to the MW accuracy of the smooth dataset, but for lower concentrations, the accuracy decreased significantly; see Figure 5 (blue circles). For the lowest concentrations (0.5 and 0.25 mg/mL), about 2% of the predictions were negative or very close to zero, i.e., the NN failed to produce an MW estimate; without these outliers, the average relative errors were 9.5% (0.5 mg/mL) and 18% (0.25 mg/mL).

Surprisingly, the NN trained to predict D_{max} on noise-free data produced almost random outputs when applied to data with noise. Even for the 16 mg/mL test data, the number of negative predictions was 17%, and the rest had an average relative D_{max} error of 15%. For the lower concentrations, the predictions were practically uncorrelated with the ground truth values.

We have retrained both NNs using the noise-augmented training set. This led to a significant improvement of the MW predictions for lower concentrations c < 4 mg/mL (see Figure 5, orange circles), and there were no negative output values (i.e., failures). For simulated concentrations ≥1 mg/mL, the accuracy of prediction was below 3%. The D_{max} predictions became reliable as well with less than 1% of failures and average errors below 3.3% for the concentrations higher than 1 mg/mL; at 0.25 mg/mL the average error was 5.8% (which was comparable to the performance of the MW NN) and 2% of failures.

Similarly, we trained the NNs on noise-augmented data simulated from IDPs and nucleic acids. To benchmark our results, we applied the NNs and the conventional methods implemented in ATSAS 3.0 (Manalastas-Cantos et al., 2021) to the noise-augmented test sets. The all-to-all comparison is presented in Figure 6, where it is seen that the NNs not only outperform the con-

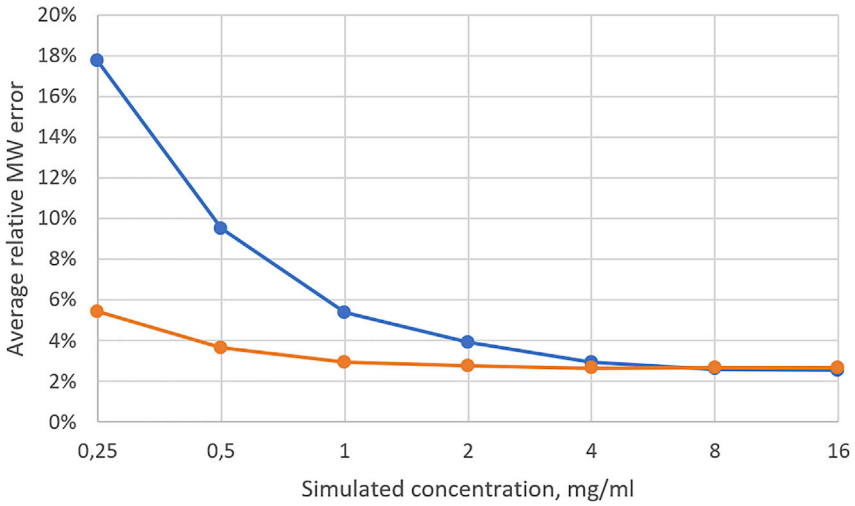

Figure 5. Performance of neural networks trained to predict molecular weight on smooth data (blue circles) and trained on noise-augmented data (orange circles) applied to the noise-augmented test set

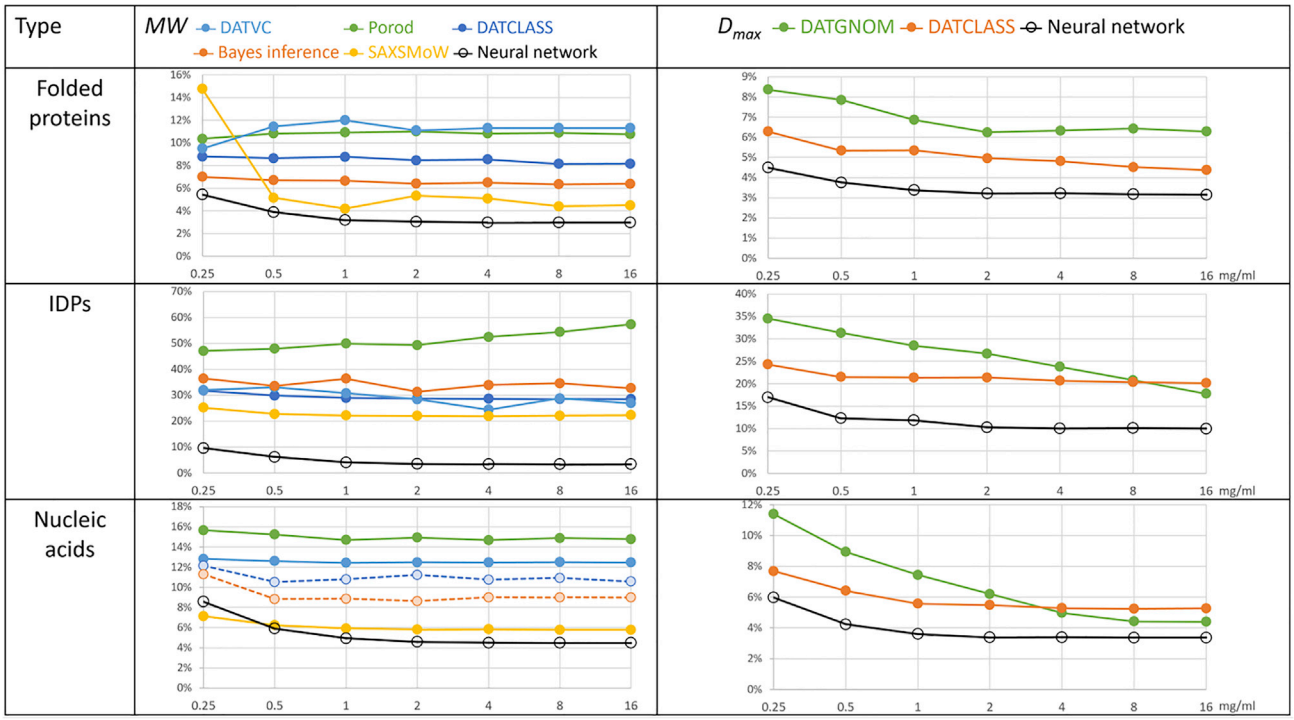

Figure 6. Average relative errors of the molecular weight (MW, left) and maximum intraparticle distance (Dmax, right) predictions for folded proteins (top), intrinsically disordered proteins (IDPs, middle), and nucleic acids (RNA and DNA, bottom) versus simulated concentration

Comparison of conventional methods (colored circles/lines) with the NNs predictions (black circles/lines). Dashed lines represent methods not directly applicable for estimating MW from nucleic acids data.

ventional methods for all types of particles but are also more robust against simulated noise. Indeed, the prediction accuracy by NNs for both MW and D_{max} improves gradually with the simulated concentration and reaches a plateau at concentrations above 1 mg/mL.

Overall, IDPs happened to be the most challenging objects for predictions. The conventional methods failed to produce reasonable MW estimates with the $<\Delta_{rel}>$ in the range of 20%–50%, while the NN showed much better results of 3%–10%, enabling to reliably estimate the MW of IDPs from SAXS data.

As a note, conventional methods for MW estimation were developed for proteins and are thus not directly applicable to data from nucleic acids. In the case of Vc method, we have used the empirically determined coefficients (Equation 7) reported by Rambo and Tainer (2013). Based on our training set, we have also established empirical correction factors for MW estimation for nucleic acids for Porod's method and SAXSMoW.

Application on experimental data

To evaluate the performance of our approach for experimental data, one requires the SAXS data collected from well-characterized monodisperse solutions with reliably determined MW and D_{max} as "ground truth" values. For folded proteins, we used data from 29 SASBDB (Kikhney et al., 2019) entries that were tagged "Benchmark" and, with a few exceptions, fitted by atomic models. The "ground truth" MW values were calculated from the protein sequence, the "ground truth" D_{max} values were obtained from the models. The NNs were retrained using the same training set but on the shortest common experimental data angular range of the SASBDB-deposited data, namely $0.02 < s < 0.3$ Å^{-1}.

The average relative MW and D_{max} errors were 10% and 7%. We have inspected the cases where the predictions were the least accurate. In the case of apoferritin, the MW was underestimated by 22%, which was expected because the MW of apoferritin (479 kDa) is beyond the range of the training set (up to 410 kDa). In the case of ribonuclease (16.5 kDa), the MW was underestimated by 30%, and D_{max} was overestimated by 11% because a large part of the protein (17% in sequence) is flexible and not present in the model (PDB: 3MZQ). The detailed results are summarized in Table S1.

To study the reproducibility of MW and D_{max} predictions from experimental data, we used 100 background-subtracted data sets from bovine serum albumin (BSA), entry SASBDB: SASDDN3 (Franke et al., 2018). The data were collected at the EMBL P12 beam line (Blanchet et al., 2015) from 2.25 mg/mL solution of BSA, exposure time 50 ms. For MW the obtained average prediction was 73.8 kDa, standard deviation 2.3 kDa, and for D_{max} the average was 108 Å and the standard deviation 4 Å. The determined values somewhat exceed those expected for a monomeric protein in agreement with the fact that the BSA sample reveals a partial dimerization in solution, as indicated by Franke et al. (2018).

Current limitations and perspectives

The present approach works only for macromolecules within the MW and D_{max} ranges covered by the training sets. The predicted

values might become meaningless if the NN fails to make a reasonable prediction, e.g., if the input data are too different from the training set. One could further expand the applicability of the trained NNs by scaling the input data angular range and adjusting the predicted parameters accordingly.

Several approaches can be used to expand the applicability of the approach. First, to generalize the applications to experimental data, the NNs can be pre-trained using several typical angular ranges, so the most suitable network can be automatically employed for the given experimental dataset. Moreover, the basis for "ground truth" can be further extended. Here, we have used only experimentally determined models of proteins and nucleic acids. It is possible to further enhance the folded proteins training set by using models computed by AlphaFold (Jumper et al., 2021) or other structure prediction approaches; the IDPs training set is amendable, e.g., by RANCH (Tria et al., 2015). Similarly, one may generate training sets for the models of folded proteins containing significant proportions of flexible chains (see the above case of ribonuclease). The extension of the nucleic acids training set is possible by using software for secondary (e.g., Mfold; Zuker, 2003) and tertiary (e.g., OligoAnalyzer; Owczarzy et al., 2008) structure predictions.

To estimate the confidence intervals of the predicted values, one could apply an ensemble of independently trained NNs or snapshots of a single NN, converging to several local minima along its optimization path (Huang et al., 2017). Alternatively, one may determine the variability of the predicted values by re-sampling the input data (i.e., adding pseudo experimental noise) using DATRESAMPLE (Manalastas-Cantos et al., 2021).

To further expand the applicability of NNs to experimental data on systems with significant interaction effects, one could augment the training set by simulating the structure factor, adding systematic noise, or simulating polydispersity.

Conclusions

We presented a method for the estimation of primary SAXS parameters using NNs. A comparison with existing methods applicable to folded proteins demonstrated that the NN approach provides higher accuracy and is robust against noise. The NN method is not restricted by assumptions (e.g., homogeneity of the electron density), and it does therefore allow one to further reassess the real capacities of SAXS data in terms of information content and to improve the accuracy of primary SAXS data analysis beyond the commonly accepted uncertainty (e.g., about 10% for MW).

To the best of our knowledge, our method is the only available approach to reliably estimate the MW from the SAXS data by IDP and nucleic acids. The D_{max} estimations by our method do not require the analysis by IFT and can therefore be conducted directly from experimental data.

STAR★METHODS

Detailed methods are provided in the online version of this paper and include the following:

- KEY RESOURCES TABLE
- RESOURCE AVAILABILITY
  - Lead contact
  - Materials availability
  - Data and code availability
- EXPERIMENTAL MODEL AND SUBJECT DETAILS
- METHODS DETAILS
  - Dataset
  - Data processing
  - Model training
- QUANTIFICATION AND STATISTICAL ANALYSIS

SUPPLEMENTAL INFORMATION

Supplemental information can be found online at https://doi.org/10.1016/j.str.2022.03.011.

ACKNOWLEDGMENTS

The work was supported by the BMBF grant 16QK10A (SAS-BSOFT). D.M. and A.K. would like to thank https://youtube.com/user/djnatron for the soundtrack.

AUTHOR CONTRIBUTIONS

D.S.M and A.G.K: conceptualization, methodology, formal analysis, software, writing original draft. D.I.S.: funding acquisition, resources, supervision, review and editing of the original draft.

DECLARATION OF INTERESTS

The authors declare no competing interests.

Received: August 11, 2021
Revised: January 24, 2022
Accepted: March 16, 2022
Published: April 11, 2022

REFERENCES

Abadi, M., Barham, P., Chen, J., Chen, Z., Davis, A., Dean, J., Devin, M., Ghemawat, S., Irving, G., Isard, M., et al. (2016). TensorFlow: a system for large-scale machine learning, 12th {USENIX} symposium on operating systems design and implementation. OSDI *16*, 265–283.

Armenteros, J.J.A., Salvatore, M., Emanuelsson, O., Winther, O., Von Heijne, G., Elofsson, A., and Nielsen, H. (2019). Detecting sequence signals in targeting peptides using deep learning. Life Sci. Alliance *2*, e201900429.

Barberato, C., Henri, M., Koch, J., Svergun, D., Barberato, C., and Koch, M.H.J. (1995). CRYSOL-a program to evaluate X-ray solution scattering of biological macromolecules from atomic coordinates. Artic. J. Appl. Crystallogr. *28*, 768–773.

Berman, H.M., Westbrook, J., Feng, Z., Gilliland, G., Bhat, T.N., Weissig, H., Shindyalov, I.N., and Bourne, P.E. (2000). The protein data bank. Nucleic Acids Res. *28*, 235–242.

Blanchet, C.E., Spilotros, A., Schwemmer, F., Graewert, M.A., Kikhney, A., Jeffries, C.M., Franke, D., Mark, D., Zengerle, R., Cipriani, F., et al. (2015). Versatile sample environments and automation for biological solution X-ray scattering experiments at the P12 beamline (PETRA III, DESY). J. Appl. Crystallogr. *48*, 431–443.

Coimbatore Narayanan, B., Westbrook, J., Ghosh, S., Petrov, A.I., Sweeney, B., Zirbel, C.L., Leontis, N.B., and Berman, H.M. (2014). The Nucleic Acid Database: new features and capabilities. Nucleic Acids Res. *42*, D114–D122.

Debye, P. (1915). Zerstreuung von Röntgenstrahlen. Ann. Phys. *351*, 809–823.

Fischer, H., De Oliveira Neto, M., Napolitano, H.B., Polikarpov, I., and Craievich, A.F. (2010). Determination of the molecular weight of proteins in solution from a single small-angle X-ray scattering measurement on a relative scale. J. Appl. Crystallogr. *43*, 101–109.

Franke, D., Jeffries, C.M., and Svergun, D.I. (2018). Machine learning methods for X-ray scattering data analysis from biomacromolecular solutions. Biophys. J. *114*, 2485–2492.

Glatter, O. (1977). Data evaluation in small angle scattering: calculation of the radial electron density distribution by means of indirect Fourier transformation. Acta Phys. Aus. *47*, 83–102.

Gräwert, T.W., and Svergun, D.I. (2020). Structural modeling using solution small-angle X-ray scattering (SAXS). J. Mol. Biol. *432*, 3078–3092.

Guinier, André, and Fournet, Gérard (1955). Small-angle Scattering of X-Rays (Wiley).

Hajizadeh, N.R., Franke, D., Jeffries, C.M., and Svergun, D.I. (2018). Consensus Bayesian assessment of protein molecular mass from solution X-ray scattering data. Sci. Rep. *8*, 1–13.

He, H., Liu, C., and Liu, H. (2020). Model reconstruction from small-angle X-ray scattering data using deep learning methods. IScience *23*, 100906.

Hopkins, J.B., Gillilan, R.E., and Skou, S. (2017). BioXTAS RAW: improvements to a free open-source program for small-angle X-ray scattering data reduction and analysis. J. Appl. Crystallogr. *50*, 1545–1553.

Huang, G., Li, Y., Pleiss, G., Liu, Z., Hopcroft, J.E., and Weinberger, K.Q. (2017). Snapshot ensembles: train 1, get M for free. Preprint at arXiv *1704.00109*. https://doi.org/10.48550/arXiv.1704.00109.

Jumper, J., Evans, R., Pritzel, A., and Green, T. (2021). Highly accurate protein structure prediction with AlphaFold. Nature, 1–11.

Kikhney, A.G., Borges, C.R., Molodenskiy, S., Jeffries, C.M., and Svergun, D.I. (2019). SASBDB: towards an automatically curated and validated repository for biological scattering data. Protein Sci. *29*, 66–75.

Kikhney, A.G., Panjkovich, A., Sokolova, A.V., and Svergun, D.I. (2016). DARA: a web server for rapid search of structural neighbours using solution small angle X-ray scattering data. Bioinformatics *32*, 616–618.

Lazar, T., Martínez-Pérez, E., Quaglia, F., Hatos, A., Chemes, L.B., Iserte, J.A., Méndez, N.A., Garrone, N.A., Saldaño, T.E., Marchetti, J., et al. (2021). PED in 2021: a major update of the protein ensemble database for intrinsically disordered proteins. Nucleic Acids Res. *49*, D404–D411.

Liu, H., Hexemer, A., and Zwart, P.H. (2012). The Small Angle Scattering ToolBox (SASTBX): an open-source software for biomolecular small-angle scattering. J. Appl. Crystallogr. *45*, 587–593.

Manalastas-Cantos, K., Konarev, P.V., Hajizadeh, N.R., Kikhney, A.G., Petoukhov, M.V., Molodenskiy, D.S., Panjkovich, A., Mertens, H.D.T., Gruzinov, A., Borges, C., et al. (2021). ATSAS 3.0: expanded functionality and new tools for small-angle scattering data analysis. J. Appl. Crystallogr. *54*, 343–355.

Mylonas, E., and Svergun, D.I. (2007). Accuracy of molecular mass determination of proteins in solution by small-angle X-ray scattering. J. Appl. Crystallogr. *40*, s245–s249.

Owczarzy, R., Tataurov, A.V., Wu, Y., Manthey, J.A., McQuisten, K.A., Almabrazi, H.G., Pedersen, K.F., Lin, Y., Garretson, J., McEntaggart, N.O., et al. (2008). IDT SciTools: a suite for analysis and design of nucleic acid oligomers. Nucleic Acids Res. *36*, W163–W169.

Petoukhov, M.V., Franke, D., Shkumatov, A.V., Tria, G., Kikhney, A.G., Gajda, M., Gorba, C., Mertens, H.D.T., Konarev, P.V., and Svergun, D.I. (2012). New developments in the ATSAS program package for small-angle scattering data analysis. J. Appl. Crystallogr. *45*, 342–350.

Petoukhov, M.V., Konarev, P.V., Kikhney, A.G., and Svergun, D.I. (2007). ATSAS 2.1 – towards automated and web-supported small-angle scattering data analysis. J. Appl. Crystallogr. *40*, s223–s228.

Piiadov, V., Ares de Araújo, E., Oliveira Neto, M., Craievich, A.F., and Polikarpov, I. (2019). SAXSMoW 2.0: online calculator of the molecular weight of proteins in dilute solution from experimental SAXS data measured on a relative scale. Protein Sci. *28*, 454–463.

Porod, G. (1951). Die Röntgenkleinwinkelstreuung von dichtgepackten kolloiden Systemen. Kolloid-Zeitschrift *124*, 83–114.

Rambo, R.P., and Tainer, J.A. (2013). Accurate assessment of mass, models and resolution by small-angle scattering. Nature *496*, 477–481.

Schmidhuber, J. (2015). Deep Learning in neural networks: an overview. Neural Networks *61*, 85–117.

Svergun, D., Koch, M., Timmins, P., and May, R. (2013). Small Angle X-Ray and Neutron Scattering from Solutions of Biological Macromolecules (Oxford University Press).

Svergun, D.I. (1992). Determination of the regularization parameter in indirect-transform methods using perceptual criteria. J. Appl. Cryst. *25*, 495–503.

Tange, Ole (2018). GNU Parallel 2018 (Ole Tange). https://dx.doi.org/10.5281/zenodo.1146014.

Tikhonov, A.N., and Arsenin, V.Y. (1977). Solutions of Ill-Posed Problems, *1* (Winston), p. 487.7.

Tria, G., Mertens, H.D.T., Kachala, M., and Svergun, D.I. (2015). Advanced ensemble modelling of flexible macromolecules using X-ray solution scattering. IUCrJ *2*, 207–217.

Vestergaard, B., and Hansen, S. (2006). Application of Bayesian analysis to indirect Fourier transformation in small-angle scattering. J. Appl. Crystallogr. *39*, 797–804.

Zuker, M. (2003). Mfold web server for nucleic acid folding and hybridization prediction. Nucleic Acids Res. *31*, 3406–3415.

STAR★METHODS

KEY RESOURCES TABLE

REAGENT or RESOURCE	SOURCE	IDENTIFIER
Deposited data		
Raw and analyzed data	This paper	https://oc.embl.de/index.php/s/fdisAFWzws0nkW9
Software and algorithms		
TensorFlow	N/A	https://github.com/tensorflow/tensorflow
ATSAS	Manalastas-Cantos et al., 2021	https://www.embl-hamburg.de/biosaxs/download.html
GNU Parallel	Tange, 2018	https://www.gnu.org/software/parallel/
Gnnom	This paper	https://github.com/emblsaxs/gnnom
Gnnom web server	This paper	https://dara.embl-hamburg.de/mwdmax.php

RESOURCE AVAILABILITY

Lead contact

Further information and requests for resources should be directed to and will be fulfilled by the lead contact, Dmitry Molodenskiy (dmolodenskiy@embl-hamburg.de)

Materials availability

This study did not generate new unique reagents

Data and code availability

- This paper analyzes existing, publicly available data from PDB, PED and NDB databases. The data reported in this paper is publicly available as of the date of publication (https://oc.embl.de/index.php/s/fdisAFWzws0nkW9), the link to the data is listed in the KRT.
- All original code has been deposited at GitHub and is publicly available as of the date of publication (https://github.com/emblsaxs/gnnom). The GitHub link is listed in the KRT.
- A web implementation is available at (https://dara.embl-hamburg.de/mwdmax.php) which is free for academic use and does not require registration.
- Any additional information required to reanalyze the data reported in this paper is available from the lead contact upon request.

EXPERIMENTAL MODEL AND SUBJECT DETAILS

All data are generated from the dataset provided in the KRT.

METHODS DETAILS

Dataset

To create a comprehensive dataset, we selected 6588 models of folded proteins, 10089 models of intrinsically disordered proteins, and 2864 of DNA and RNA models from three sources: PDB (Berman et al., 2000), PED (Lazar et al., 2021), and the NDB server (Coimbatore Narayanan et al., 2014).

Two parameters were used to ensure equal distribution of models by MW and R_g. Different MW values guarantee that the models are of various sizes, whereas different R_g values yield various shapes, ranging from highly compact to very extended forms. In principle, the D_{max} could be used instead of R_g, however, R_g, being an integral parameter, may better ensure the coverage of the conformational space.

The algorithm for the subset selection was implemented as a Python script and is available along with the links to the utilized datasets at the GitHub. We manually filtered the data and chose the range of the training set parameters MW and D_{max} based on experimental data from SASBDB data bank (Kikhney et al., 2020). The file names of the training/validation/test datasets correspond to the

accession codes assigned in PDB and PED databases, and the full names of original PDB files are reported in the CRYSOL log files.

To test the method on experimental data, we used "Benchmark" data from SASBDB (Kikhney et al., 2020). The "ground truth" MW values were calculated from the deposited protein sequence, the "ground truth" D_{max} values were calculated directly from the models. The NNs were retrained using the same training set but on the shortest common experimental data angular range of the SASBDB-deposited data, namely $0.02 < s < 0.3$ Å^{-1}. The results and comparison of predictions with other methods are presented in Table S1.

Data processing

Simulated SAXS patterns, as well as the "ground truth" values for MW and D_{max}, were generated by the CRYSOL program (Barberato et al., 1995). The maximum number of 99 spherical harmonics was used to generate SAXS patterns of 256 points on the angular range of $0 < s < 1$ Å^{-1}.

To augment the data with a realistic experimental noise, we used a homemade Python script available at the GitHub (https://github.com/emblsaxs/gnnom/blob/master/gnnom/pytools/augment_with_buffer.py).

Model training

All models were trained on a desktop PC (Intel Core CPU 2.60GHz 12 Cores) using GPU (NVIDIA GeForce RTX 2060) and the TensorFlow package. For all models, architecture and hyper-parameters were optimized by minimizing the respective loss function. The complexity of the NN architecture was reduced step by step until it worsened the resulting loss function. The NNs contained an input layer of 256 points and 3 hidden layers of 80 units, resulting in 32960 parameters. The 'tanh' was used as an activation function for all layers, 'mean absolute percentage error' as a loss function with 'adam' optimizer and L2 kernel regularizer. The regularizer was used to smooth the weights of the NNs units and to reduce overfitting.

QUANTIFICATION AND STATISTICAL ANALYSIS

This study did not use statistical analysis. All experimental details can be found in the STAR Methods section.